Microfluidic chaotic stirrer utilizing induced-charge electro-osmosis

Hui Zhao and Haim H. Bau*

Department of Mechanical Engineering and Applied Mechanics, University of Pennsylvania, Philadelphia, Pennsylvania 19104, USA

(Received 22 February 2007; published 28 June 2007)

Recently, there has been a growing interest in using induced electro-osmosis to pump fluids in microfluidic devices. We show that induced electroosmosis can also be used to promote stirring and chaotic advection. To this end, we study theoretically a stirrer in which the flow patterns are alternated in time. We first analyze an idealized embodiment of the stirrer that admits a simple analytical solution for the flow patterns. The stirrer consists of a concentric annulus whose outer surface is defined by an array of electrodes that provide a spatially varying potential distribution. The resulting electric field induces quadruple electro-osmotic flow around the inner cylinder. By timewise alternating the potential distribution around the outer cylinder, we induce chaotic advection in the cavity. Subsequently, we carry out numerical simulations for a more realistic design that can be readily constructed, and demonstrate that it is possible to induce chaotic advection also in this case.

DOI: 10.1103/PhysRevE.75.066217 PACS number(s): 47.52.+j, 47.65.−d, 47.63.mf

I. INTRODUCTION

Recently, the use of induced (ac) electro-osmosis has been proposed as an effective means to pump fluids in microfluidic systems [1–8]. Induced electro-osmosis is distinct from the classical electro-osmosis [9,10], since it results from the interaction between the electric field and ions in the electric double layer formed by the polarizing effect of the electric field itself. The intensity of the resulting flow is proportional to the square of the electric field intensity. At relatively low frequencies, the direction of the electric body force is independent of the direction of the electric field. Thus, unidirectional fluid motion can be induced with ac fields, thus avoiding many of the complications associated with dc electric fields, such as electrode electrochemistry.

The phenomenon of induced-charge electro-osmosis around conducting particles has been studied extensively [7,11–18] Only recently has it been recognized that, in the absence of symmetry, induced electro-osmosis leads to net pumping in conduits [1,16,19] and net forces on particles [19–22].

Since the Reynolds numbers are typically very low and the flow is laminar, fluid mixing is a significant challenge in microfluidic systems [23]. Aref [24] demonstrated that, when flow patterns form closed orbits, one can induce Lagrangian chaos and effective stirring by alternating periodically between two or more flow patterns. See also Ottino [25] for a lucid review. In this paper, we demonstrate that induced electro-osmosis can be used to generate various flow patterns and chaotic advection. In the first part of the paper, we present an idealized model which allows us to obtain exact expressions for the flow patterns. The stirrer consists of a concentric annulus. The outer surface of the cylinder consists of an electrode (or an array of electrodes) that forms a spatially varying potential. The inner cylinder is conducting. As a result of the induced electric double layer around the inner cylinder, convective cells form in the annulus. By timewise alternations of the electric potential of the outer cylinder, we induce chaotic advection in the annulus. Although the above stirrer design exhibits the basic physics of the process, it is not readily amenable for fabrication. Therefore, in the second part of the paper, we analyze a more realistic device that can be readily constructed.

II. MATHEMATICAL MODEL

We start with a simple embodiment of the stirrer. Consider a concentric annulus. The radii of the inner and outer cylinders are, respectively, a and $a+b$. The annulus is filled with electrolyte solution of bulk concentration C_0 and dielectric constant ϵ. The inner cylinder is electrically conducting. The outer cylinder is subjected to a potential distribution $f(\theta)$. We use the cylindrical coordinate system $\{r,\theta\}$ with its origin at the center of the inner cylinder (Fig. 1). When the inner, conducting cylinder is subjected to an electric field, it polarizes. The induced surface charges attract counterions from the electrolyte solution, which, in turn, leads to the formation of an electric double layer. The thickness of the double layer is the Debye screening length

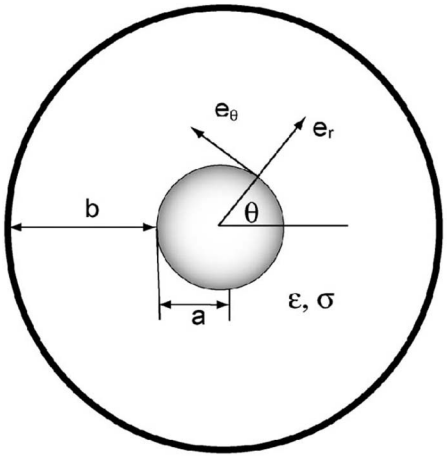

FIG. 1. Schematic depiction of a stirrer consisting of a concentric annulus of inner radius a and outer radius $a+b$.

*Author to whom correspondence should be addressed. Electronic address: bau@seas.upenn.edu

$\lambda_D = \sqrt{\epsilon RT/(2F^2C_0)}$, where R is the ideal gas constant, T is the absolute temperature, and F is the Faraday constant. When $C_0 = 10$ mM, $\lambda_D \sim 8$ nm. We assume that $b \sim 100$ μm, $b/\lambda_D \sim 125$, and one can use the thin electric layer approximation.

The electrolyte solution is treated as a conductor, and the electrical potential in the solution satisfies the Laplace equation

$$\nabla^2 \phi = 0. \tag{1}$$

We assume that the electric field is too small to induce Faradaic reactions on the inner cylinder's surface. Thus, at equilibrium, no current enters the double layer, and on the inner cylinder's surface $(r=a)$

$$\vec{n} \cdot \vec{\nabla} \phi = 0. \tag{2}$$

In the above, $\vec{n}$ is the outer normal vector to the surface. On the outer cylinder's surface, we impose a potential distribution of the form

$$\phi(r+b, \theta) = f(\theta). \tag{3}$$

We assume that Faradaic reactions take place at the surface of the outer cylinder and that the electrical resistance of the electric double layer is relatively small so that there is a small difference between the electrode's potential and the potential immediately outside the electric double layer.

Since typically the Reynolds number associated with the electrokinetic flow is very small, the fluid motion can be described with the Stokes equation

$$-\vec{\nabla} p + \mu \nabla^2 \vec{u} = \vec{0} \tag{4}$$

and the continuity equation

$$\vec{\nabla} \cdot \vec{u} = 0. \tag{5}$$

In the limit of the thin-double-layer approximation, the electric field is coupled with the flow problem through the Smoluchowski slip velocity [7],

$$\vec{u}(a, \theta) = -\frac{\epsilon \phi(a, \theta)}{\mu} \vec{\nabla}_t \phi(a, \theta). \tag{6}$$

In the above, $\vec{\nabla}_t \phi$ is the tangential component of the potential's gradient. Equation (6) is applicable as long as the ζ potential is not too large, i.e., on the order of the thermal voltage ($\sim$25 mV) or smaller [26,27].

We assume that the potential of the outer cylinder varies slowly, and we neglect induced electroosmotic flow at the surface of the outer cylinder:

$$\vec{u}(a+b, \theta) = \vec{0}. \tag{7}$$

When the approximation (7) is not applicable, one can readily determine the flow field induced by the electroosmotic flow at the outer cylinder and superimpose it on the flow fields computed later in this paper.

It is convenient to nondimensionalize the various variables. We use the radius of the inner cylinder a as the length scale; $\epsilon(\Delta\phi_0)^2/(\mu a)$ as the velocity scale; and $\mu a^2/(\epsilon \Delta \phi_0^2)$ as the time scale. In the above, $\Delta\phi_0 = \max f(\theta) - \min f(\theta)$. We define the dimensionless radius $\rho = r/a$ and the annulus aspect ratio $\xi = b/a$. $1 < \rho < 1 + \xi$.

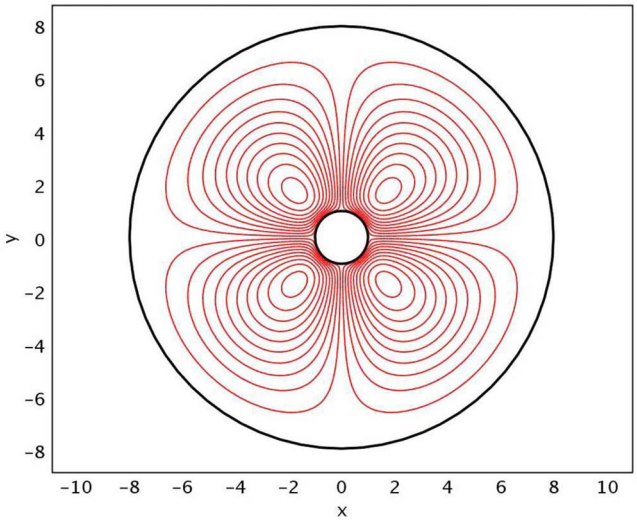

FIG. 2. (Color online) Flow field (streamlines) resulting from induced electro-osmosis around the inner cylinder. The potential distribution $A \sin\theta$ is imposed on the outer cylinder.

For concreteness, we consider the case of the electrical potential on the outer cylinder given by

$$f(\theta) = A \sin(\theta + \theta_0). \tag{8}$$

The electrical potential is

$$\phi = A \frac{1+\xi}{1+(1+\xi)^2} \left(\rho + \frac{1}{\rho}\right) \sin(\theta + \theta_0). \tag{9}$$

To calculate the velocity field, we introduce the stream function Ψ. Ψ satisfies the biharmonic equation

$$\nabla^4 \Psi = 0. \tag{10}$$

The velocity components are related to Ψ by

$$u_r = \frac{1}{r} \frac{\partial \Psi}{\partial \theta}, \quad u_\theta = -\frac{\partial \Psi}{\partial r}. \tag{11}$$

The boundary conditions on the outer and inner cylinders are given by the nonslip condition and the Smoluchowski formula (6), respectively. The general solution for the stream function has the form

$$\Psi(r, \theta) = \left(\frac{A_1}{r^2} + B_1 + C_1 r^2 + D_1 r^4\right) \sin 2(\theta + \theta_0). \tag{12}$$

The constants A_1, B_1, C_1, and D_1 are determined by using the appropriate boundary conditions.

Figure 2 depicts the flow pattern when $\theta_0 = 0$ and $\xi = 8$. The flow consists of four counter-rotating vortices. Although the flow is effective in moving material across the width of the annulus, the flow is laminar and a poor mixer. This shortcoming can be overcome with the use of chaotic advection.

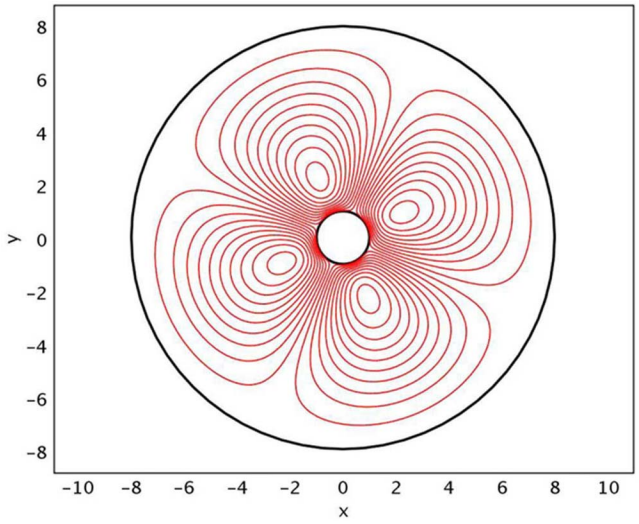

FIG. 3. (Color online) Flow field (streamlines) resulting from superimposing flow patterns A ($\theta_0=0$) and B ($\theta_0=\pi/4$).

III. AN IDEALIZED CHAOTIC STIRRER

Aref [24] demonstrated that, by alternating between two (or more) different closed-orbit patterns A and B, one can generate Lagrangian chaos. Here, we obtain two such patterns by timewise alternations of the potential imposed on the outer cylinder. In the time interval $kT<t<kT+T/2$, we impose the potential (8) with phase angle $\theta_0=0$ on the outer electrode. We refer to the corresponding flow field as pattern A. In the time interval $kT+T/2<t<(k+1)T$, we impose the potential (8) with phase angle $\theta_0=\pi/4$. We refer to the corresponding flow field as pattern B. The time period T is much larger than any of the other time constants associated with the various physical processes that occur in the annulus, such as the time constant associated with the charging of the double layer.

We examine the performance of the stirrer by tracking the trajectories of passive tracer particles:

$$\frac{d\vec{r}}{dt} = f_A(t)\vec{u}_A + f_B(t)\vec{u}_B. \tag{13}$$

In the above,

$$f_A(t) = \begin{cases} 1 & \text{when} \quad kT < t < kT + /T/2, \\ 0 & \text{when} \quad kT + T/2 < t < (k+1)T, \end{cases} \tag{14}$$

$$f_B(t) = \begin{cases} 0 & \text{when} \quad kT < t < kT + /T/2, \\ 1 & \text{when} \quad kT + T/2 < t < (k+1)T, \end{cases} \tag{15}$$

and the subscripts A and B denote, respectively, flow patterns A and B. At time $t=0$, the particle is located at $\vec{r}_0$. T is the switching time period. $k=0,1,2,3,\ldots$ is an integer.

The ordinary differential equations (13) with the initial condition $\vec{r}_0$ are nonlinear. We solve these equations with a fourth-order Runge-Kutta algorithm (MATLAB program ODE45). We find it convenient to summarize the computational results in the form of stroboscopic images (Poincaré sections). The Poincaré section consists of a record of the passive tracer particles' locations at the end of each period T, i.e., $\{r(kT),\theta(kT)\}$, $k=0,1,2,\ldots$. When the pattern in the Poincaré sections is regular and smooth, it implies that the streamlines have a simple geometric character and the stirring is poor. When the pattern of the Poincaré sections is irregular and no or just a few closed trajectories are traced, the flow is deemed to be chaotic and provides good stirring.

Figure 3 depicts the streamlines in the limit of high-frequency switching $T\to 0$. The two flow patterns superimpose to form a well-organized flow. As the period of alternations increases so does the complexity of the flow.

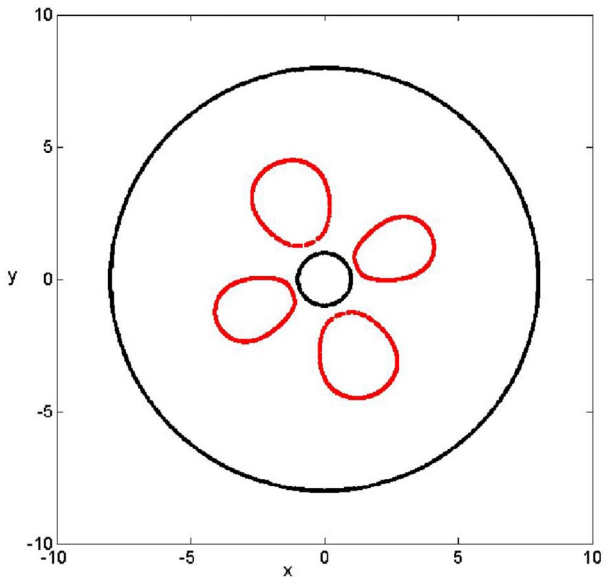

FIG. 4. (Color online) Stroboscopic image (Poincaré section) of the trajectory of four passive tracer particles initially positioned at $r(0)=1.82$, and $\theta(0)=0$, $\pi/2$, π, and $3\pi/2$. $T=2$. 5000 periods are recorded.

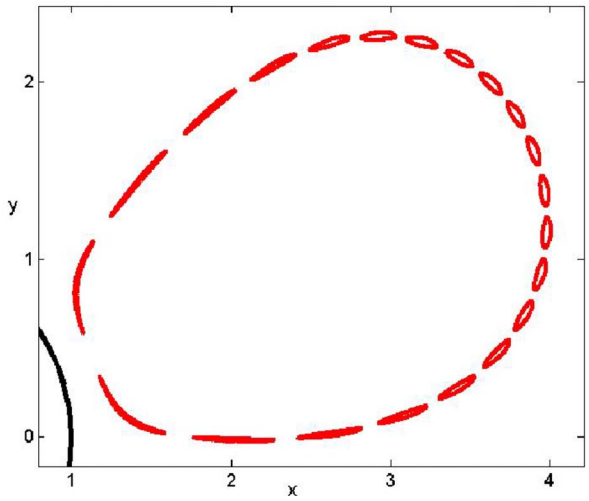

FIG. 5. (Color online) Enlarged stroboscopic image (Poincaré section) of the trajectory of a passive tracer particle initially positioned at $(r,\theta)=(1.82,0)$. $T=4$. 5000 periods are recorded.

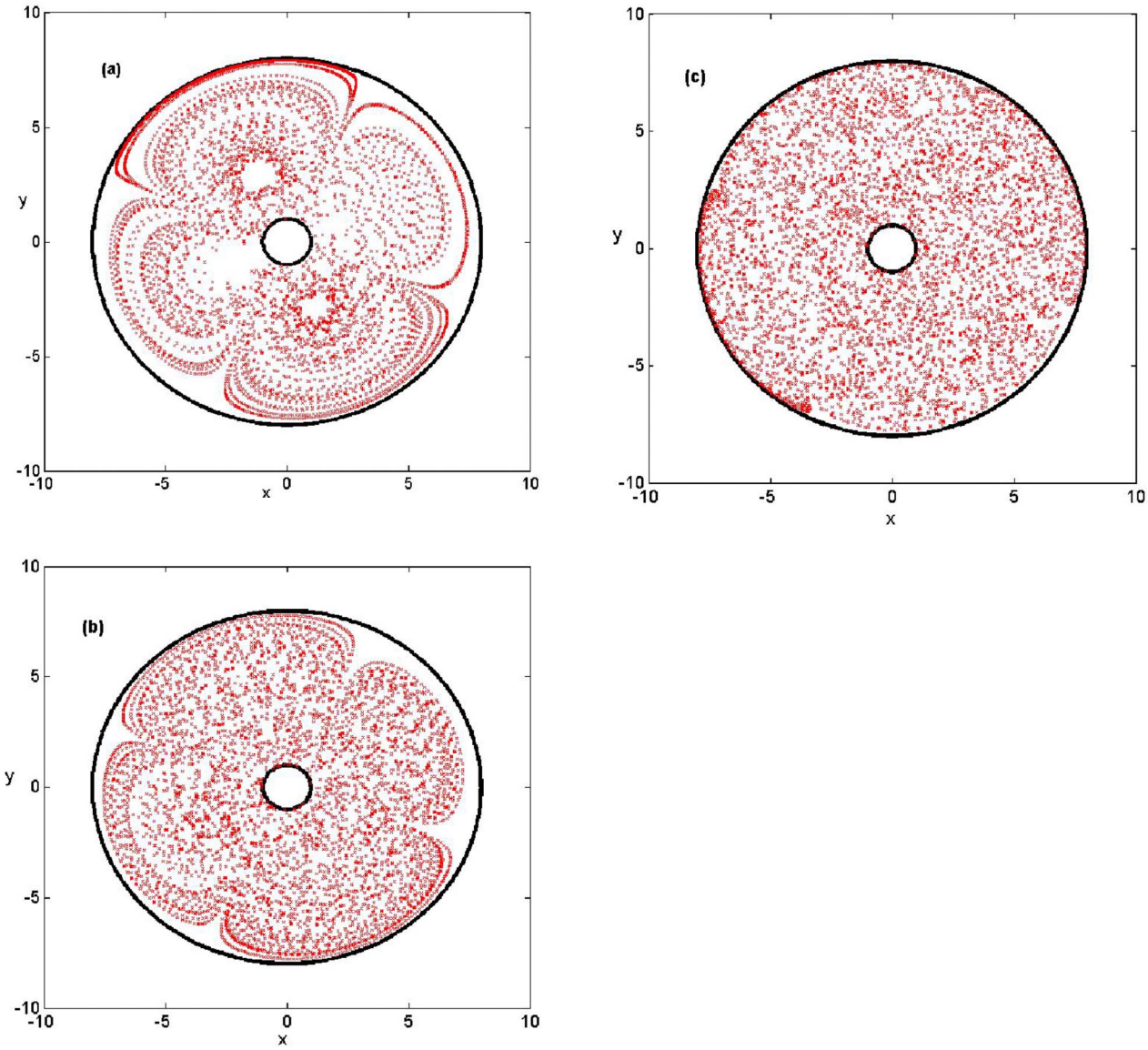

FIG. 6. (Color online) Stroboscopic image (Poincaré section) of the trajectory of a passive tracer particle initially positioned at $(r,\theta)=(1.82,0)$. $T=$(a) 10, (b) 20, and (c) 100. 5000 periods are recorded.

Figure 4 depicts the Poincaré sections, when $T=2$ and the four passive tracer particles are initially located at $\{r(0),\theta(0)\}=(1.82,0)$, $(1.82,\pi/2)$, $(1.82,\pi)$, and $(1.82,3\pi/2)$. The figure records 5000 periods. The stroboscopic image consists of a closed orbit, indicating that the dynamical system has two noncommensurate periods.

Figure 5 depicts an enlarged section of the stroboscopic image (Poincaré section) when $T=4$. Consistent with the Poincaré-Birkhoff theorem, the tori deform significantly and form a "petal" structure that leads in the Poincaré section to a sequence of hyperbolic (saddle) and elliptic fixed points.

Figures 6(a)–6(c) depict, respectively, the stroboscopic images (Poincaré sections) when $T=10$ (a), 20 (b), and 100 (c). Witness that, as the period T increases, the chaotic regions increase in size and the tracer particles visit all regions of the annulus.

Another diagnostic tool often used to examine the effect of the stirrer in enhancing mixing [24] consists of tracking the deformation of a material blob. To this end, we inserted the material blob at $\sqrt{10}-0.1<r<\sqrt{10}+0.1$, $-\pi/60<\theta<\pi/60$. Figure 7 depicts the positions of 10^4 particles initially located in the blob at $t=0,3T,5T,7T,9T,11T,13T,40T$. In the above, $T=20$. Witness that the material blob undergoes a sequence of stretching and folding until the material spreads to cover the entire volume of the cavity.

In the above, we presented a simple paradigm of a chaotic stirrer in which fluid flow is driven by induced electroosmosis. The example was deliberately designed with mathematical convenience in mind. In the next section, we illustrate that similar ideas can be put into use in a device that can be readily fabricated.

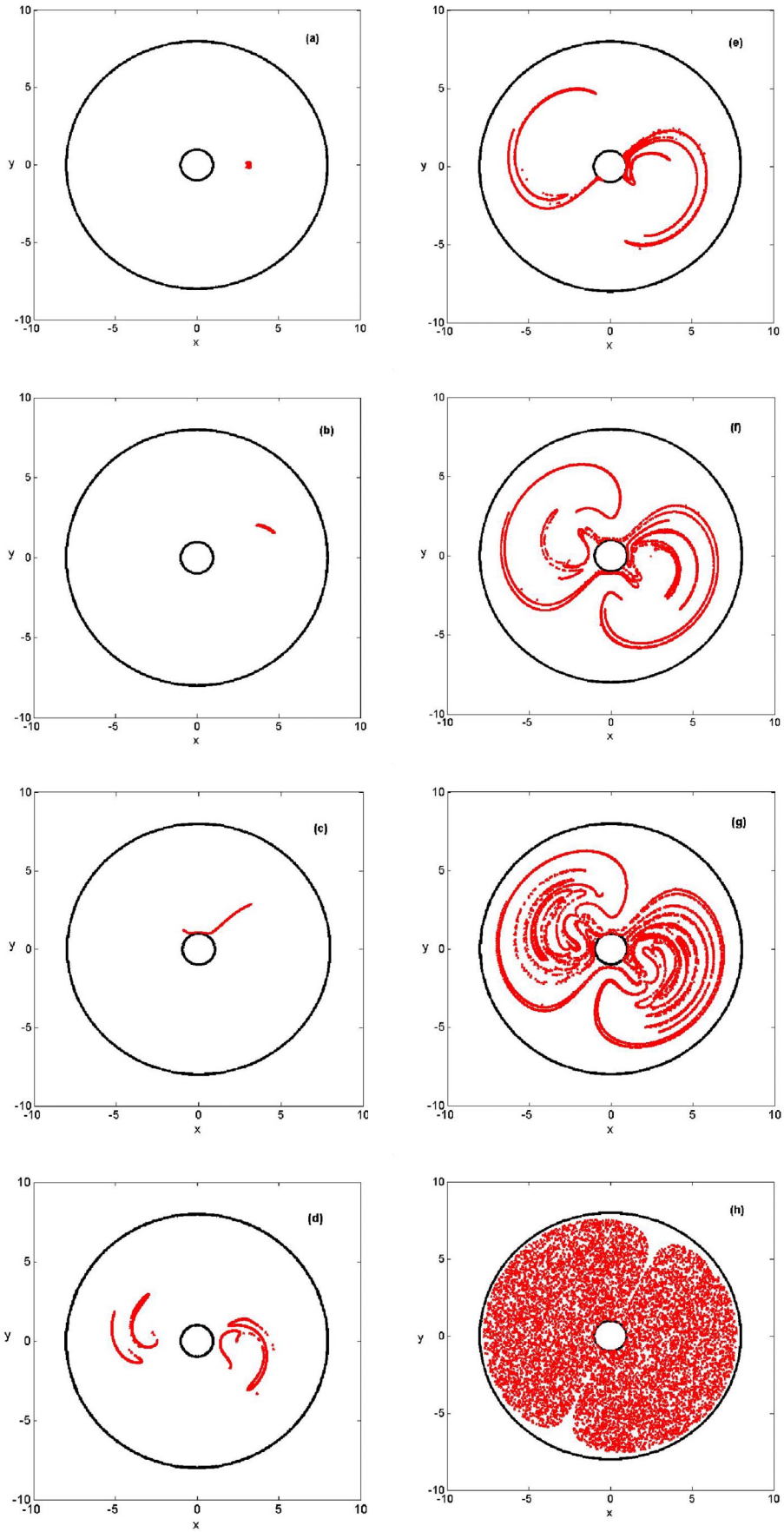

FIG. 7. (Color online) Trajectory of a material blob initially located at $\sqrt{10}-0.1<r<\sqrt{10}+0.1$, $-\pi/60<\theta<\pi/60$, when $t=0$ (a), $3T$ (b), $5T$ (c), $7T$ (d), $9T$ (e), $11T$ (f), $13T$ (g), and $40T$ (h). $T=20$.

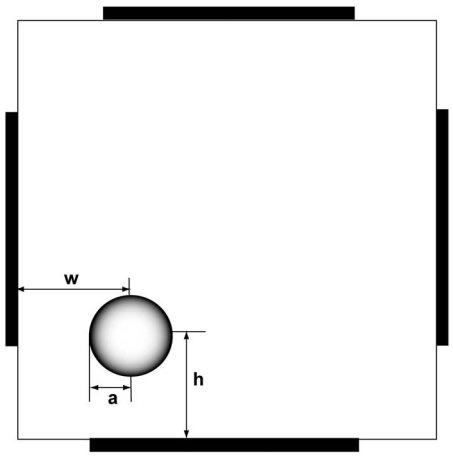

FIG. 8. Schematic depiction of the second stirrer's geometry consisting of a conducting cylinder placed off center in a square cavity. Electrodes are deposited along the edges of the box.

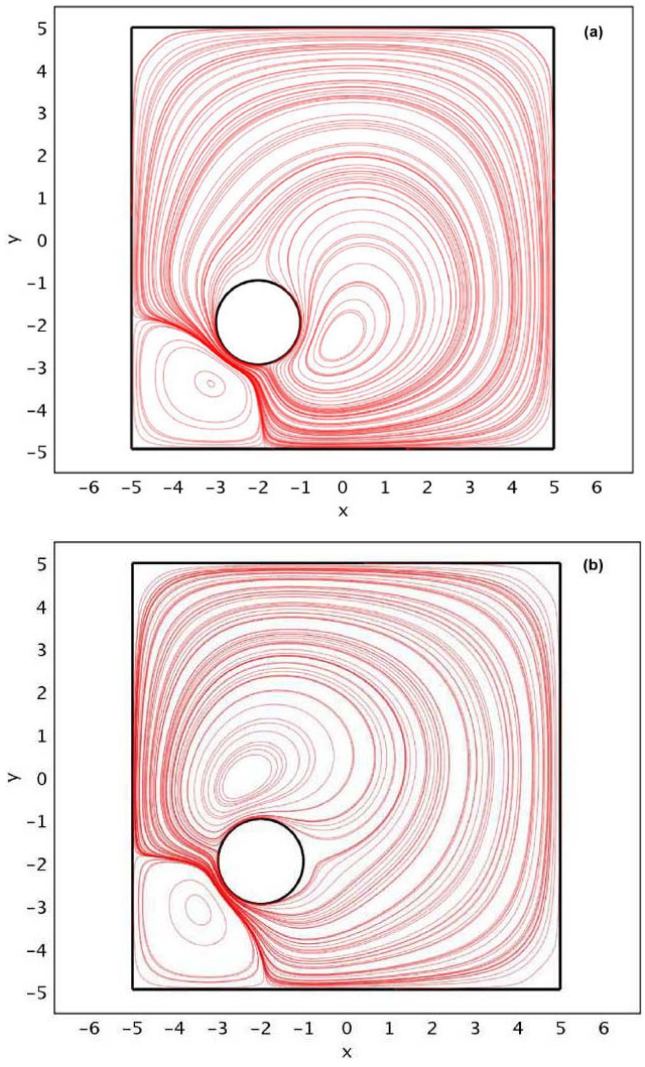

FIG. 9. (Color online) Flow pattern A (a) occurs when the top and the bottom electrodes are active and flow pattern B (b) occurs when the left and the right electrodes are active.

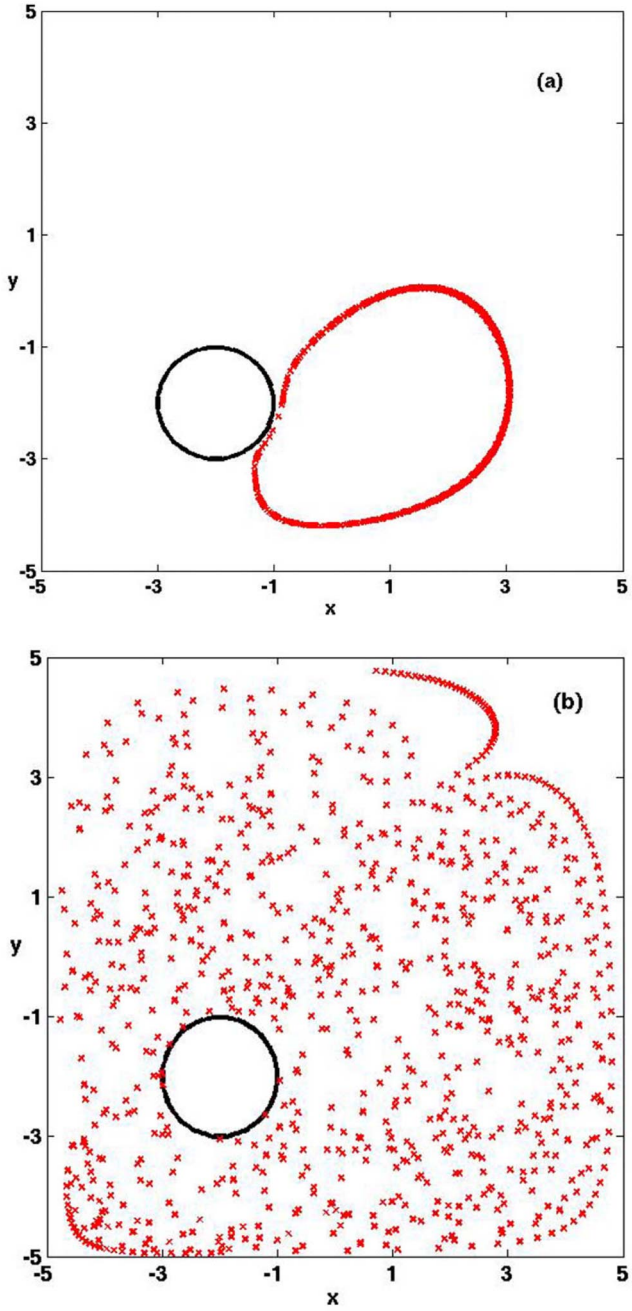

FIG. 10. (Color online) Stroboscopic images (Poincaré sections) of the trajectory of a passive trace particle initially located at $(x,y)=(2,0)$ when $T=1$ (a) and 16 (b). 2000 periods are recorded.

IV. A PRACTICAL CHAOTIC STIRRER

Our previous example required one to impose a spatially distributed potential on the outer surface of the stirrer. Such a task may not be easy. In this section, we describe a device that can be readily fabricated. We need, however, to resort to numerical techniques to calculate the flow patterns.

Consider a conducting cylinder of radius a located at the left bottom corner of a closed square cavity, distance h above the bottom and distance w from the left edge (Fig. 8). The edge length of the box is $10a$. The cavity is filled with electrolyte solution of permittivity ϵ and conductivity σ. Four

electrodes, each with length $6a$, are deposited along the cavity's edges (heavy lines in Fig. 8). The electrodes' centers are at the centers of the edges. Only two of the electrodes are active at any given time. We obtain flow pattern A when voltage V_0 is imposed on the bottom electrode and voltage $-V_0$ on the top electrodes; and we get flow pattern B when potential V_0 is imposed on the left electrode and potential $-V_0$ on the right electrode. The conducting cylinder was intentionally placed off the cavity's center to allow the formation of two distinct flow fields when the two electrode pairs are actuated.

The momentum and electrical equations and the corresponding boundary conditions are the same as in Sec. II. The inactive electrodes act like conductors with floating potentials (that need to be determined). We specify on the passive electrodes that

$$\phi = \text{const} \quad \text{and} \quad \int_A \frac{\partial \phi}{\partial n} dA = 0. \tag{16}$$

Due to the complex geometry, analytical solutions are not possible. Instead, we use the finite element software COMSOL 3.2 to calculate the electrical potentials and the velocity fields A and B. Once the velocity fields have been computed, we use the kinetic equations to trace the trajectories of passive tracer particles. To capture the motion accurately, we use a very fine grid. Figures 9(a) and 9(b) depict flow pattern A (when the bottom and top electrodes are active) and flow pattern B (when the left and right electrodes are on).

Figures 10(a) and 10(b) depict the stroboscopic images (Poincaré sections) of a passive tracer particle initially located at $(x,y)=(2,0)$ when $T=1$ (a) and 16 (b), respectively. These figures are a record of 2000 periods. As in Sec. III, as the period increases so does the complexity of the flow. This section demonstrates that chaotic advection can be obtained in an embodiment of a stirrer that can be readily fabricated.

V. CONCLUSION

Two examples of chaotic stirrers in which fluid flow was driven by induced electro-osmosis were presented. The stirrers do not require any moving parts and are suitable for applications in microfluidics. The first paradigm consisted of a stirrer in the shape of a concentric annulus with the outer cylindrical surface forming an electrode with spatially and temporarily controlled potential distribution. The simple geometry allowed us to obtain analytical solutions for the flow fields and investigate in detail the trajectories of passive tracer particles as functions of the period of time alternations of the electrode's potential. As the period of alternations increased so did the complexity of the flow. At sufficiently high periods, the stirrer exhibited chaotic advection and a passive tracer particle visited nearly the entire volume of the stirrer's cavity.

Since, in practice, it may not be easy to spatially control the electrode's potential distribution, we investigated a second paradigm of a stirrer consisting of a conducting cylinder placed off center in a square cavity equipped with two electrode pairs stretched along the outer surfaces of the cavities. Only one pair of electrodes was active at any given point in time. Two different flow patterns were formed by alternately activating the two pairs of electrodes. Due to the complexity of the geometry, these flow patterns were computed numerically with finite elements. By switching periodically between the two pairs of electrodes, the complexity of the flow increased until chaotic advection ensued as in the first embodiment of the stirrer.

The paper demonstrates that induced electro-osmosis can be used to facilitate stirring. The stirrer has the advantage of simple design and requires only low voltage for operation. The stirrers presented in this paper consisted of a single, cylindrically shaped conducting internal structure. The design can be extended to include arrays of internal structures—each inducing electro-osmotic flow in its vicinity. Another interesting possible extension of the work is the optimization of the stirrer's geometry to maximize stirring efficiency.

ACKNOWLEDGMENTS

The work was supported, in part, by the Nano/Bio Interface Center (NSF NSEC Grant No. DMR-0425780) and by NSF NIRT Grant No. CBET-0609062.

[1] A. Ramos, H. Morgan, N. G. Green, A. Gonzalez, and A. Castellanos, J. Appl. Phys. **97**, 084906 (2005).
[2] N. G. Green, A. Ramos, A. Gonzalez, H. Morgan, and A. Castellanos, Phys. Rev. E **61**, 4011 (2000).
[3] N. G. Green, A. Ramos, A. Gonzalez, H. Morgan, and A. Castellanos, Phys. Rev. E **66**, 026305 (2002).
[4] A. Gonzalez, A. Ramos, N. G. Green, A. Castellanos, and H. Morgan, Phys. Rev. E **61**, 4019 (2000).
[5] M. Z. Bazant and Y. X. Ben, Lab Chip **6**, 1455 (2006).
[6] J. P. Urbanski, T. Thorsen, J. A. Levitan, and M. Z. Bazant, Appl. Phys. Lett. **89**, 143508 (2006).
[7] T. M. Squires and M. Z. Bazant, J. Fluid Mech. **509**, 217 (2004).
[8] L. H. Olesen, H. Bruus, and A. Ajdari, Phys. Rev. E **73**, 056313 (2006).
[9] R. J. Hunter, *Foundations of Colloid Science* (Oxford University Press, New York, 2001).
[10] J. Lyklema, *Fundamentals of Interface and Colloid Science*. Vol. 2: *Solid-Liquid Interfaces* (Academic Press, San Diego, CA, 1995).
[11] A. S. Dukhin, Colloid J. USSR **48**, 376 (1986).
[12] A. S. Dukhin and V. R. Murtsovkin, Colloid J. USSR **48**, 203 (1986).
[13] N. I. Gamayunov, G. I. Mantrov, and V. A. Murtsovkin, Colloid J. **54**, 20 (1992).
[14] N. I. Gamayunov, V. A. Murtsovkin, and A. S. Dukhin, Colloid

J. USSR **48**, 197 (1986).
[15] V. A. Murtsovkin, Colloid J. **58**, 358 (1996).
[16] M. Z. Bazant and T. M. Squires, Phys. Rev. Lett. **92**, 066101 (2004).
[17] J. A. Levitan, S. Devasenathipathy, V. Studer, Y. X. Ben, T. Thorsen, T. M. Squires, and M. Z. Bazant, Colloids Surf., A **267**, 122 (2005).
[18] T. S. Simonova, V. N. Shilov, and O. A. Shramko, Colloid J. **63**, 114 (2001).
[19] T. M. Squires and M. Z. Bazant, J. Fluid Mech. **560**, 65 (2006).
[20] E. Yariv, Phys. Fluids **17**, 051702 (2005).
[21] D. Saintillan, E. Darve, and E. S. G. Shaqfeh, J. Fluid Mech. **563**, 223 (2006).
[22] H. Zhao and H. H. Bau, Langmuir **23**, 4053 (2007).
[23] H. A. Stone, A. D. Stroock, and A. Ajdari, Annu. Rev. Fluid Mech. **36**, 381 (2004).
[24] H. Aref, J. Fluid Mech. **143**, 1 (1984).
[25] J. M. Ottino, *Kinematics of Mixing: Stretching, Chaos and Transport* (Cambridge University Press, Cambridge, U.K., 1989).
[26] K. T. Chu and M. Z. Bazant, Phys. Rev. E **74**, 011501 (2006).
[27] M. Z. Bazant, M. S. Kilic, B. D. Storey, and A. Ajdari (unpublished).